Shape-induced pairing of spheroidal squirmers

Ruben Poehnl and William E. Uspal [*]

Department of Mechanical Engineering, University of Hawai'i at Mānoa,
2540 Dole Street, Holmes Hall 302, Honolulu, Hawaii 96822, USA

The "squirmer model" is a classical hydrodynamic model for the motion of interfacially driven microswimmers, such as self-phoretic colloids or volvocine green algae. To date, most studies using the squirmer model have considered spherical particles with axisymmetric distribution of surface slip. Here, we develop a general approach to the pairing and scattering dynamics of two spheroidal squirmers. We assume that the direction of motion of the squirmers is restricted to a plane, which is approximately realized in many experimental systems. In the framework of an analytically tractable kinetic model, we predict that, for identical squirmers, an immotile "head-to-head" configuration is stable only when the particles have oblate shape and a nonaxisymmetric distribution of surface slip. We also obtain conditions for stability of a motile "head-to-tail" configuration: for instance, the two particles must have unequal self-propulsion velocities. Our analytical predictions are compared against detailed numerical calculations obtained using the boundary element method.

I. INTRODUCTION

Self-assembly [1–4], clustering [5–9], and particle motility alignment [10–14] are among the most discussed topics in the active matter community. In each of these phenomena, collective behavior emerges from nonequilibrium interactions between self-motile microscopic particles. These particles usually self-propel through liquid, making hydrodynamic interactions—interactions mediated by flow in the suspending medium—an important and ubiquitous nonequilibrium effect [15].

A broad class of synthetic and biological microswimmers propel themselves by driving flow within a thin layer at the fluid/solid interface. For instance, ciliated microorganisms are covered by a thin carpet of threadlike appendages that beat in a coordinated fashion. The squirmer model, first introduced by Lighthill [16] and Blake [17], was originally developed to describe the motion of ciliated, spherical microorganisms [18]. In the simplest version of this model, the detailed, time-dependent motion of the cilia is coarse grained as a prescribed steady tangential slip velocity. This slip velocity provides the interfacial actuation (i.e., thrust) needed for self-propulsion. Additionally, the slip velocity drives flow in the surrounding solution, leading to long-ranged hydrodynamic interactions between the squirmer and other objects in the solution. These features have made the squirmer model a popular approach for understanding the flow-mediated interactions between swimming microorganisms, as well as between microorganisms and bounding surfaces [19–25]. For instance, Ishikawa *et al.* exhaustively cataloged the collision and scattering dynamics of squirmer pairs [19]. As another example, various studies have addressed nutrient uptake (i.e., feeding) of microorganisms in the framework of the squirmer model [26,27].

---

[*]uspal@hawaii.edu

Since its original development, the squirmer model has found applications well beyond its initial purpose. For instance, synthetic active colloids driven by self-generated gradients of a thermodynamic variable (e.g., temperature, chemical potential, or electrical potential [28–31]) can often be approximated as "effective squirmers." Instead of resolving the propulsion mechanism in detail, a slip velocity on the surface of the particle is prescribed [32]. The slip determines two major swimming properties, speed U_s and stresslet $\mathbf{S}$ [33,34]. As an example that justifies this approach, it was recently observed that metallodielectric Janus discoids, energized by AC fields, tend to form "head-to-head" bound pairs [35]. Modeling of the propulsion mechanism (induced charge electrophoresis [36,37]) revealed that hydrodynamic interactions dominated interactions between particles, i.e., the particles behaved as effective squirmers.

One microscopic property that has proven to be important in active matter is particle geometry [38–41]. Shape can impact the swimming speed of an active particle, the rate of working, and the flow field sourced by the particle [42–47]. Collisions between rodlike particles can lead to nematic ordering in an active suspension [48]. In view of the importance of shape, various studies have considered non-spherical squirmers–usually prolate spheroids [23,42,49,50]. For instance, Ishikawa and Hoto modeled the paramecium *P. caudatum* with a prolate spheroid actuated by interfacial slip. The slip was assumed to be a superposition of five harmonic functions of the elevation angle [51]. In an effort to fully generalize the squirmer model to both prolate and oblate spheroids, we recently developed and characterized a complete set of orthogonal, axisymmetric squirming modes in spheroidal coordinates [52]. We found that the odd-numbered squirming modes contribute to the self-propulsion velocity, while the even numbered contribute to the the stresslet.

For interfacially driven microswimmers, a second means of controlling their motion is offered by breaking symmetries of the slip velocity. This symmetry breaking can be imposed, as when a self-phoretic particle is fabricated with nonaxisymmetric surface chemistry [53,54], or can emerge *in situ*, due to effects of confinement [37,55] or symmetry-breaking fields [36,56]. So far, applications of the squirmer model have mostly been restricted to axisymmetric slip, although more general slip has been considered for spherical squirmers [57–60]. For instance, Burada *et al.* consider the far-field interaction of two spherical squirmers with a chiral distribution of slip. They find that these spheres can exhibit oscillatory "bounded states" in which they orbit around a common average trajectory [61].

II. THEORY

In this work, we develop a framework to study the consequences of particle shape and non-axisymmetry of the surface slip for interactions between interfacially-driven microswimmers. We develop analytical predictions in a far-field, "point-particle" model, building on the Saintillan-Shelley kinetic theory of microswimmers [62–65]. Our analytical predictions are supported by high resolution numerical calculations using the squirmer model, which resolve the finite size of the particle and near-field hydrodynamic interactions. We show that both nonspherical shape and breaking of the axisymmetry are necessary conditions to form stable "head-to-head" bound pairs. These immotile bound states are held together by (far-field) hydrodynamic interactions. Similarly, we find that motile "head-to-tail" bound pairs can be stable only when the particles are nonspherical (although they can be axisymmetric). Overall, we find good agreement between theory and numerics, suggesting that our framework offers a promising approach for studying self-organization in heterogeneous active suspensions.

A. Minimal model

We model swimmer $\alpha \in \{1, 2\}$ as a pointlike particle with swimming direction $\hat{d}^{(\alpha)}$ and self-propulsion velocity $U_s^{(\alpha)} \geqslant 0$. Swimmers are coupled by the flows they generate. The velocity of swimmer α is

$$\mathbf{U}^{(\alpha)} = U_s^{(\alpha)} \hat{d}^{(\alpha)} + \mathbf{u}(\mathbf{x}_\alpha). \tag{1}$$

In the second term, the swimmer is advected by the ambient flow, evaluated at its position $\mathbf{x}_\alpha$. (The finite size of the swimmer is neglected). For the rotation of the swimmer, we write the Jeffery equation [64]

$$\dot{\hat{d}}^{(\alpha)} = (\mathcal{I} - \hat{d}^{(\alpha)}\hat{d}^{(\alpha)}) \cdot (\Gamma_\alpha \mathbf{E}(\mathbf{x}_\alpha) + \mathbf{W}(\mathbf{x}_\alpha)) \cdot \hat{d}^{(\alpha)}. \tag{2}$$

Here, Γ_α is a shape parameter that is zero for a sphere, positive for a prolate spheroid that has its major axis aligned with $\hat{d}^{(\alpha)}$, and negative for an oblate spheroid that has its minor axis aligned with $\hat{d}^{(\alpha)}$. The tensors $\mathbf{E}(\mathbf{x}_\alpha)$ and $\mathbf{W}(\mathbf{x}_\alpha)$ are the rate-of-strain and vorticity, respectively, evaluated at $\mathbf{x}_\alpha$, where $\mathbf{E} = \frac{1}{2}(\nabla\mathbf{u} + \nabla\mathbf{u}^T)$ and $\mathbf{W} = \frac{1}{2}(\nabla\mathbf{u} - \nabla\mathbf{u}^T)$. $\mathcal{I}$ is the identity tensor.

To model swimmer-generated flow, we associate an active "stresslet" with each swimmer. In general, the stresslet provides the slowest decaying contribution of a force-free, rigid microswimmer to the surrounding flow field. It can be obtained from the surface traction [19,66]:

$$S_{ij}^{(\alpha)} = \frac{1}{2} \int_{\Sigma_\alpha} [\sigma_{ik}\hat{n}_k x_j + \sigma_{jk}\hat{n}_k x_i] \, dS - \frac{1}{3} \int_{\Sigma_\alpha} \sigma_{lk}\hat{n}_k x_l \, dS \, \delta_{ij}. \tag{3}$$

The integral is taken over the surface Σ_α of particle α, $\hat{n}$ points from the surface of the particle into the surrounding fluid, and $\boldsymbol{\sigma} = -p\mathcal{I} + \mu(\nabla\mathbf{u} + \nabla\mathbf{u}^T)$ is the stress tensor for a Newtonian fluid. Here, $p(\mathbf{x})$ is the pressure and μ is the dynamic viscosity of the fluid. The velocity field due to a stresslet located at the origin is given by

$$u_i = \frac{1}{8\pi\mu}\left(\frac{x_i\delta_{jk}}{r^3} - \frac{3x_i x_j x_k}{r^5}\right)S_{jk}^{(\alpha)}, \tag{4}$$

where r is distance from the origin and x_i is a location in the fluid. For a swimmer with an axisymmetric surface actuation, the stresslet can be written as [67]

$$\mathbf{S}^{(\alpha)} = \sigma_0^{(\alpha)}\left(\hat{d}^{(\alpha)}\hat{d}^{(\alpha)} - \frac{\mathcal{I}}{3}\right). \tag{5}$$

The sign of $\sigma_0^{(\alpha)}$ determines the "pusher" ($\sigma_0^{(\alpha)} < 0$) or "puller" ($\sigma_0^{(\alpha)} > 0$) character of the swimmer.

However, not all microswimmers have axisymmetric actuation. For instance, consider metallodielectric particles that are energized by an AC electric field and swim via induced charge electrophoresis (ICEP) [36]. The applied field can break axisymmetry. Thus, we consider a more general stresslet, written in a frame aligned with the principal axes $\hat{c}$, $\hat{d}$, and $\hat{e}$ of $\mathbf{S}^{(\alpha)}$:

$$\mathbf{S}^{(\alpha)} = S_{cc}^{(\alpha)}\hat{c}\hat{c} + S_{dd}^{(\alpha)}\hat{d}\hat{d} + S_{ee}^{(\alpha)}\hat{e}\hat{e}, \tag{6}$$

with $\text{tr}(\mathbf{S}^{(\alpha)}) = 0$. Since $\mathbf{S}^{(\alpha)}$ is symmetric and real-valued, its principal axes are orthogonal, and we define $\hat{c} \times \hat{d} = \hat{e}$. This form of the stresslet tensor is generic. However, for simplicity, we make the assumption that the direction of propulsion of an isolated particle is $\hat{d}$, i.e., aligned with a principal axis. This assumption is realized by an ICEP particle with spheroidal shape and axisymmetric metal coverage, swimming in unbounded solution [Fig. 1(a)]. If the electric field is in the $\hat{z}$ direction and the particle axis of symmetry is given by $\hat{d}$, the particle will rotate such that $\hat{d}$ is perpendicular to $\hat{z}$ [36,40]. After rotation, the particle will swim strictly in $\hat{d}$ with a stresslet tensor in the form of Eq. (6). A detailed technical discussion of $\mathbf{S}$ and the assumption concerning $\hat{d}$ is provided in the Supplemental Material (SM) [68]. Additionally, we note that Eq. (6) reduces to Eq. (5) when $S_{dd}^{(\alpha)} = 2\sigma_0/3$ and $S_{cc}^{(\alpha)} = S_{ee}^{(\alpha)} = -\sigma_0/3$.

In the following, we restrict our consideration to two swimmers moving in the xy plane, and study conditions for obtaining stable bound states. The instantaneous configuration of the system is specified by the center-to-center distance d and the angles ϕ_1 and ϕ_2, where ϕ_α is the angle between $\hat{d}^{(\alpha)}$ and a fixed axis, chosen as the x-axis (see Fig. 1 in the SM). We assume that $\hat{c}^{(\alpha)}$ and $\hat{d}^{(\alpha)}$ lie within the xy plane. For convenience, we specify that swimmer 1 is instantaneously at $\mathbf{x}_1 = (0, 0, 0)$. Swimmer 2 has position $\mathbf{x}_2 = (x, y, 0)$. We construct $\dot{x}$, $\dot{y}$, $\dot{\phi}_1$, and $\dot{\phi}_2$ as functions of x, y, ϕ_1, and ϕ_2, and look for fixed point configurations at which these functions evaluate to zero, representing a
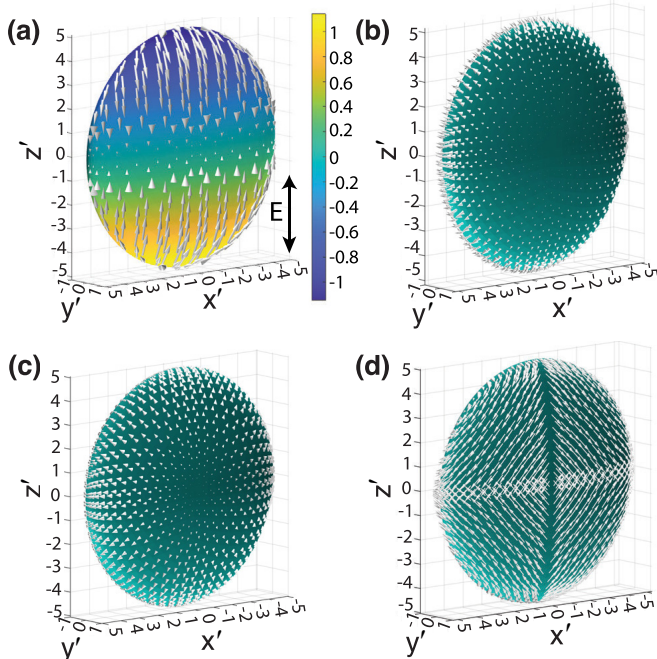
FIG. 1. (a) An oblate particle that self-propels in the presence of an AC electric field (black arrow) by ICEP. The background color indicates the electrostatic potential (arbitrary units) on the particle surface for the half-period in which the field is pointing in the positive z' direction. White arrows show the surface slip, which is nonaxisymmetric. (b) Distribution of slip for the first squirming mode B_1. (c) Distribution of slip for B_2. (d) Nonaxisymmetric slip for $\tilde{B}$, following the definition in Eq. (7). In all panels, $r_e = 5$.

bound state. For simplicity, we consider only bound states in which the propulsion axes are aligned with the center-to-center axis.

The point-particle model is analytically tractable and yields a wealth of predictions. However, we wish to compare these predictions against numerical results that account for finite size and do not truncate the particle-generated flow field to the leading-order term.

B. Squirmer model

We consider $N \in \{1, 2\}$ spheroidal particles in unbounded Newtonian fluid. Following Ref. [52], for particle α, we take the length of the semiaxis of symmetry to define $b_y^{(\alpha)}$, and the length of the other semiaxes to define $b_x^{(\alpha)}$. Thus, each particle has an aspect ratio $r_e^{(\alpha)}$ defined by $r_e \equiv b_x/b_y$, with $r_e < 1$ for a prolate spheroid, $r_e = 1$ for a sphere, and $r_e > 1$ for an oblate spheroid. The quantity Γ_α is related to $r_e^{(\alpha)}$ by $\Gamma = (1 - r_e^2)/(1 + r_e^2)$. The characteristic size of the particle, $L_0^{(\alpha)}$, is chosen as $b_y^{(\alpha)}$.

The center of particle α is located at $\mathbf{x}_\alpha$. The fluid velocity $\mathbf{u}(\mathbf{x})$ is governed by the Stokes equation $-\nabla p + \mu \nabla^2 \mathbf{u} = 0$ and the incompressibility condition $\nabla \cdot \mathbf{u} = 0$. On the surface Σ_α of particle α, the velocity obeys $\mathbf{u} = \mathbf{U}^{(\alpha)} + \mathbf{\Omega}^{(\alpha)} \times (\mathbf{x} - \mathbf{x}_\alpha) + \mathbf{v}_s^{(\alpha)}(\mathbf{x})$. Additionally, $|\mathbf{u}| \to 0$ as $|\mathbf{x}| \to \infty$. Each particle is force free and torque free: $\int_{\Sigma_\alpha} \boldsymbol{\sigma} \cdot \hat{\mathbf{n}} \, dS = 0$ and $\int_{\Sigma_\alpha} (\mathbf{x} - \mathbf{x}_\alpha) \times \boldsymbol{\sigma} \cdot \hat{\mathbf{n}} \, dS = 0$.

For each swimmer, the slip $\mathbf{v}_s^{(\alpha)}$ is fixed in a frame attached to the swimmer. It is specified via a set of squirming mode amplitudes. In previous work, we generalized the axisymmetric squirming modes to spheroidal particles. The amplitudes are denoted by $B_i^{(\alpha)}$, with $i \geqslant 1$ [52], and here are assumed to be given in units of an arbitrary characteristic velocity. The first two modes are shown

in Figs. 1(b) and 1(c). Here, in order to break axisymmetry, we develop a new squirming mode $\tilde{B}^{(\alpha)}$ inspired by the slip profile of ICEP particles. This squirming mode has slip distribution

$$
\begin{aligned}
\mathbf{v}_s^{(\alpha)}(\mathbf{x}) = \tilde{B}^{(\alpha)}[&\text{sign}(z')(\cos(\varphi)\hat{e}_\xi - \hat{e}_\varphi(\hat{e}_\xi \cdot \hat{e}_{z'})) \\
&- \text{sign}(x')(\sin(\varphi)\hat{e}_\xi - \hat{e}_\varphi(\hat{e}_\xi \cdot \hat{e}_{x'}))] \cdot H(y'),
\end{aligned}
\tag{7}
$$

shown in Fig. 1(d). Here, $H(y')$ is the step function, and $\hat{e}_\varphi$ and $\hat{e}_\xi$ are two surface tangential basis vectors in a particle-centered spheroidal coordinate system. (The prime symbol is used to distinguish the coordinate system in Fig. 1 from the coordinate system used for studying pair interactions).

We briefly discuss the properties of a single squirmer. From solution of the governing equations, we obtain U_s and $\mathbf{S}$ for a given r_e and set of squirming mode amplitudes. Due to the linearity of the Stokes equation, the contribution of each squirming mode can be calculated individually and superposed. For the axisymmetric modes, Fig. 2 in the SM shows how the B_i contribute to $U_s^{(\alpha)}$ and $\sigma_0^{(\alpha)}$. For the nonaxisymmetric mode, we show $S_{cc}^{(\alpha)}$, $S_{dd}^{(\alpha)}$, and $S_{ee}^{(\alpha)}$ as a function of r_e in Fig. 5 in the SM. This squirming mode makes no contribution to $S_{dd}^{(\alpha)}$ or $U_s^{(\alpha)}$, and contributes antisymmetrically to $S_{cc}^{(\alpha)}$ and $S_{ee}^{(\alpha)}$.

For $N = 2$, we solve for the particle velocities numerically, using the boundary element method (BEM) [69]. We obtain trajectories using a rigid body dynamics engine [42]. For simplicity, we assume that $L_0^{(1)} = L_0^{(2)}$. (The point-particle model has no inherent length scale. Since $S_{ij} \sim L_0^3$ and $U_s \sim L_0^2$ for a squirmer, differences in size can be straightforwardly accommodated in our model).

III. RESULTS

A. Head-to-head pairing

We look for fixed point solutions of the point-particle model with $(x, y, \phi_1, \phi_2) = (d_0, 0, 0, \pi)$. Through a detailed derivation in the SM, we obtain

$$
d_0 = \sqrt{\frac{-3\left(S_{dd}^{(1)} + S_{dd}^{(2)}\right)}{8\pi\mu\left(U_s^{(1)} + U_s^{(2)}\right)}}.
\tag{8}
$$

Given that $U_s^{(\alpha)} > 0$, to obtain a finite separation $d > 0$, it is required that $(S_{dd}^{(1)} + S_{dd}^{(2)}) < 0$. In other words, the pair must have a net "pusher" character. In the SM, we present a general linear stability analysis. Here, we discuss identical swimmers, i.e., $U_s^{(1)} = U_s^{(2)}$, $\mathbf{S}^{(1)} = \mathbf{S}^{(2)}$, and $\Gamma_1 = \Gamma_2$. As conditions for stability, we obtain $\Gamma < -1/3$ and $[S_{cc}(-1 + \Gamma) + S_{dd}(1 + 2\Gamma)][S_{cc}(-1 + \Gamma) - S_{dd}(1 + 4\Gamma)] < 0$, given that $S_{dd} < 0$. Notably, the requirement $\Gamma < -1/3$ corresponds to an oblate shape, recalling the discoidal particles in Ref. [35]. Intriguingly, head-to-head pairing cannot be obtained for axisymmetric swimmers [Eq. (5)]. For $S_{dd} = 2\sigma_0/3$ and $S_{cc} = S_{ee} = -\sigma_0/3$, with $\sigma_0 < 0$, the second condition reduces to $\Gamma > -1/9$. This cannot be reconciled with $\Gamma < -1/3$. Thus, this work completes the analysis of Ref. [35], which assumed an axisymmetric stresslet. Here, we have shown that nonaxisymmetry is a necessary ingredient in the pairing observed in Ref. [35].

To further investigate deviation from axisymmetry, we consider stresslets of the form

$$
\mathbf{S} = \mathbf{S}_{ax} + \sigma_0 \delta(\hat{c}\hat{c} - \hat{e}\hat{e}),
\tag{9}
$$

where $\mathbf{S}_{ax}$ is equal to the right hand side of Eq. (5), and δ is dimensionless. We obtain $\Gamma < -1/3$ and $(-1 + 3\Gamma(-3 + \delta) - 3\delta)(1 + \Gamma + \delta(-1 + \Gamma)) < 0$. Notably, these requirements are independent of σ_0 and U_s. In Fig. 2(a), the background color shows the predicted phase map. We also show two types of numerical data. Crosses represent squirmers with a nonaxisymmetric squirming mode. This mode introduces the perturbation δ in a controllable manner (see Fig. 5 in the SM). Circles show the results for an effective squirmer model for ICEP particles. Red symbols indicate pairs without a stable bound state. The theoretical and numerical results largely agree with each other. The one area of significant mismatch is for $\Gamma \approx -1$, i.e., oblate spheroids with large r_e. Recalling that b_y was
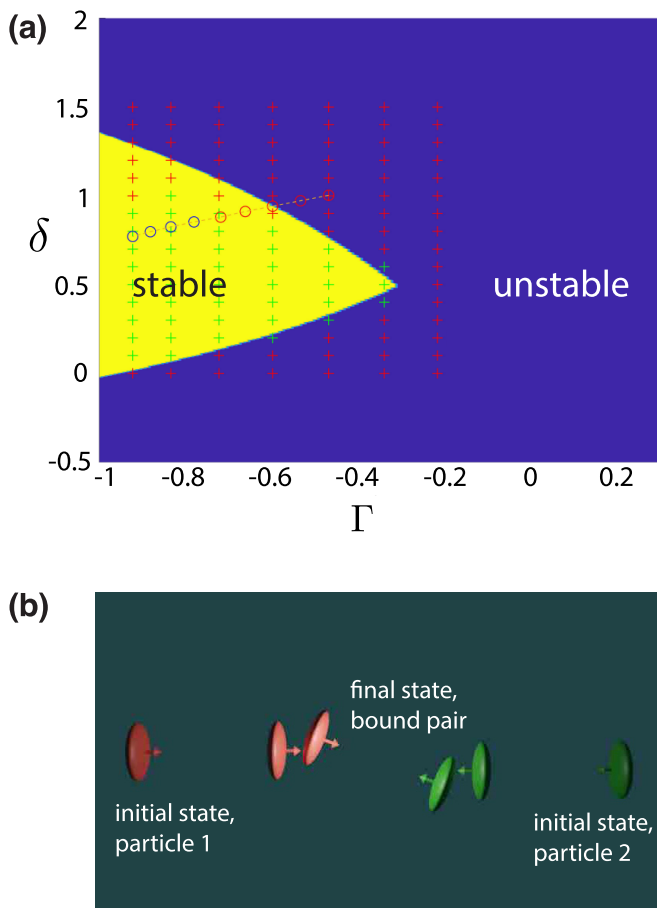
FIG. 2. (a) Phase map for head-to-head pairs. The background colors show the stability predicted by the analytical model. Crosses represent the results of numerical calculations for nonaxisymmetric squirmers [Eq. (7)] with modes $B_1^{(\alpha)} = 0.1$, $B_2^{(\alpha)} = -1$ and varying $\tilde{B}$ and Γ. Circles indicate numerical data for the ICEP effective squirmer model, and are connected by a line to guide the eye. Green and blue symbols indicate pairs with with a stable bound state; red symbols represent unstable pairs. (b) Trajectory obtained for $\Gamma = -0.835$ and $\tilde{B} = 1.68$.

chosen as a characteristic length, oblate particles with large r_e also have large b_x. When $b_x \gg d_0$, the point particle assumption is expected to be erroneous. In Fig. 2(b), we show pair formation for $\Gamma = -0.835$ and $\tilde{B} = 1.68$.

The condition $\Gamma < -1/3$ has a straightforward physical interpretation. At the location of a particle, the rate-of-strain tensor $\mathbf{E}$ has two principal axes. Spheroidal particles tend to align their long axes with the local axis of extension [70,71]. For an axisymmetric stresslet [Eq. (5)] located at the origin and oriented in the x direction, we evaluate $\mathbf{E}_{ax}$ at the position $x = d$, $y = 0$. From the eigenvalues and eigenvectors of this quantity, we find that the axis of extension is indeed in the y direction. Thus, the straining component of flow will tend to stabilize the orientation of oblate spheroids in a head-on collision. Furthermore, we note that δ does not appear in the condition $\Gamma < -1/3$. As a consistency check, we form the rate-of-strain tensor $\mathbf{E}_\delta$ for the nonaxisymmetric contribution to flow [the second term in Eq. (9)], assuming that $\hat{d} = \hat{x}$ and $\hat{c} = -\hat{y}$. We find that it indeed evaluates to zero at $x = d$, $y = 0$. Additionally, in Fig. 3(a), we plot the flow from the
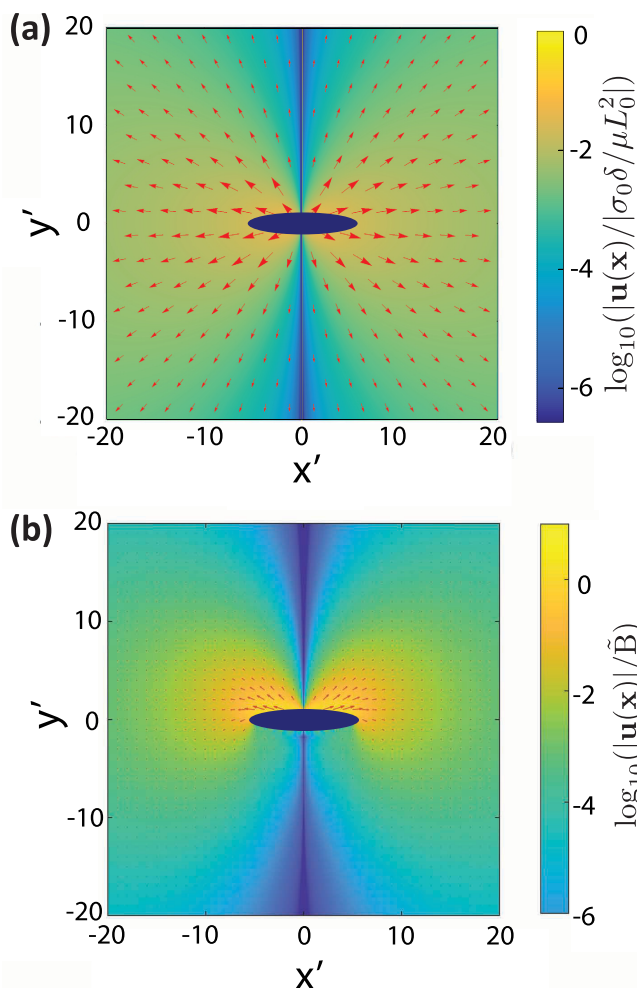
FIG. 3. (a) Flow field due to a nonaxisymmetric stresslet located at the origin, with $\hat{c}$ in the x' direction and $\hat{e}$ in the z' direction. The direction of the flow is shown for the case $\sigma_0\delta < 0$. The flow is radially outward, but the magnitude is anisotropic. An oblate spheroid is shown for comparison with (b). (b) Flow field due to the nonaxisymmetric $\tilde{B}$ mode for the oblate spheroidal particle shown in Fig. 1(d). In both (a) and (b), the flow velocity is zero at $x' = 0$.

idealized nonaxisymmetric stresslet. On the $\hat{d}$ axis (in the figure, the y' axis), it evaluates to zero, which explains why d_0 is determined by the axisymmetric component of the stresslet [Eq. (8)].

The second requirement for linear stability, $(-1 + 3\Gamma(-3 + \delta) - 3\delta)(1 + \Gamma + \delta(-1 + \Gamma)) < 0$, is more difficult to interpret. The quantities Γ and δ are implicated, both individually and as a product with each other. Additionally, by introducing dummy variables into the Jacobian, we have confirmed that both vorticity and transverse advection (i.e., motion in y, transverse to the center-to-center vector) contribute to this condition. Some insight can be obtained from the form of the Jacobian in Eq. (40) of the SM. The stresslet component S_{cc} appears only in off-diagonal terms that couple transversal displacements and particle rotations. This suggests that the nonaxisymmetric stresslet is important in the intricate dance in which particles simultaneously rotate to face each other and slide laterally into register, as shown in Fig. 2(b). In contrast, it is known that spherical squirmers in a head-on collision are unstable to maneuvering past each other in a process involving
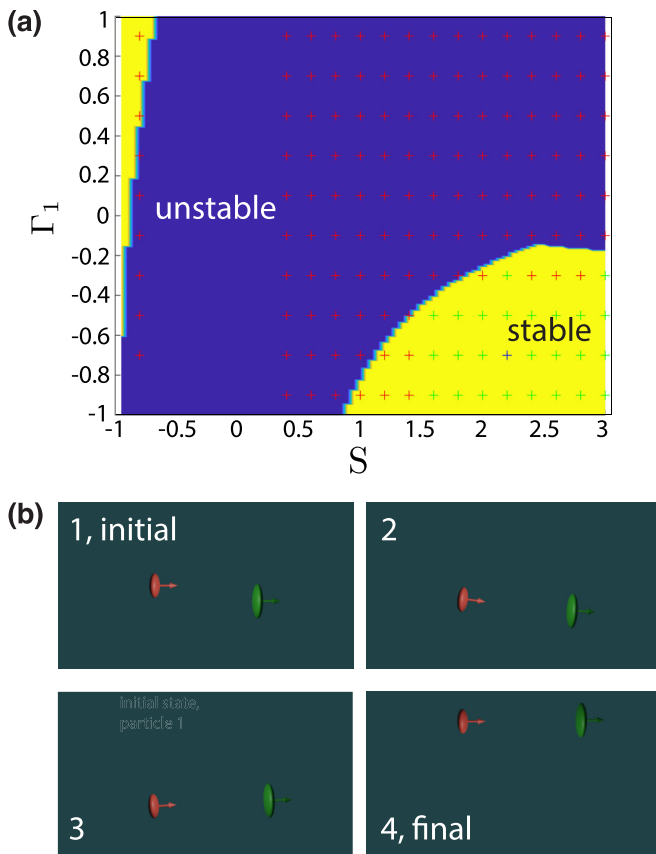
FIG. 4. (a) Phase map for head-to-tail pairs with $\Gamma_2 = -0.8$ and $V = 0.8$, and varying S and Γ_1. The background colors show the stability predicted by our model and symbols represent the results of numerical calculations. Green and blue symbols indicate pairs with a stable bound state; red symbols indicate pairs without a stable bound state. (b) Snapshots of an example trajectory for $S = 2.2$ and $\Gamma_1 = -0.7$. This pair is represented by a blue cross in (a). The particles are initially separated by $x_{2,\text{initial}} = 3$ and $y_{2,\text{initial}} = 20$.

rotations and transversal motion [35]. Looking at the flow for the nonaxisymmetric stresslet in Fig. 3(a), some stabilizing roles of this radially outward flow may be in hindering the particles from moving past each other and in contributing to alignment. Regarding alignment, we recall that the magnitude and sign of the contribution of the rate-of-strain tensor to rotation is controlled by the shape parameter Γ [Eq. (2)]. We also note that while the flow fields close to the particle can differ significantly between the idealized nonaxisymmetric stresslet in Fig. 3(a) and the nonaxisymmetric squirming mode in Fig. 3(b), far from the particle, both flow fields are radially outward.

B. Head-to-tail pairs

Now we look for fixed point solutions with $(x, y, \phi_1, \phi_2) = (d_0, 0, 0, 0)$. We obtain

$$d_0 = \sqrt{\frac{3\left(S_{dd}^{(1)} + S_{dd}^{(2)}\right)}{8\pi\mu\left(U_s^{(2)} - U_s^{(1)}\right)}}. \tag{10}$$

Notably, the two particles must have unequal speeds U_s for $d_0 > 0$. The bound pair moves with a steady speed given by Eq. (27) in the SM. Regarding stability against displacements in x, we again

obtain the "net pusher" condition $(S_{dd}^{(1)} + S_{dd}^{(2)}) < 0$. From Eq. (10), this implies $U_s^{(1)} > U_s^{(2)}$. The other stability conditions are $S_{dd}^{(2)}(1 + 3\Gamma_1) + S_{dd}^{(1)}(1 + \Gamma_2) > 0$ and Eq. (48) in the SM. For axisymmetric swimmers, we can obtain stable pairing. Specifically, $\sigma_0^{(1)} + \sigma_0^{(2)} + 3(\sigma_0^{(2)}\Gamma_1 + \sigma_0^{(1)}\Gamma_2) > 0$ and Eq. (13) in the SM. Overall, the phase behavior is determined by four parameters: Γ_1, Γ_2, $S \equiv \sigma_0^{(2)}/\sigma_0^{(1)}$, and $V \equiv U_s^{(2)}/U_s^{(1)}$. For the slice of phase space in Fig. 4(a), we fix $V = 0.8$ and $\Gamma_2 = -0.8$, but vary Γ_1 and S. In the numerics, B_1 and B_2 are chosen to vary S while keeping $V = 0.8$. The model has good agreement with the numerics. There are two areas of significant disagreement. Similar to head-to-head pairs, one is for oblate particles with large r_e. The other is the slim area bordering $S = -1$, where $d_0 \to 0$. An example trajectory is shown in Fig. 4(b).

IV. CONCLUSIONS

We have shown that nonspherical active particles can form bound pairs through far-field hydrodynamic interactions (Fig. 5). A surprising finding of our work is that squirmers with nonaxisymmetric surface slip may be capable of pairing behaviors that are not obtainable for squirmers with axisymmetric slip.

We restricted our consideration to swimmers moving in the plane containing their center-to-center vector (the xy plane). For nonaxisymmetric particles defined by Eq. (9), a $90°$ rotation of both particles around their $\hat{d}$ axes will invert the sign of δ. Therefore, when head-to-head bound states, aligned with x, are stable against perturbations in the xy plane, they will be unstable in the yz plane. However, our quasi-2D assumption is realized in most active matter experiments. For head-to-tail pairs of axisymmetric particles, the stability conditions found here apply to general three-dimensional motions.

Future work could incorporate the effects of inertia and/or near-field hydrodynamic interactions [25,72]. Lubrication interactions can induce bound states for spherical squirmers near contact [21,25]. Additionally, making use of the Faxén relations for spheroids would account for the finite size of a particle in its response to ambient flow [66,73]. Our model may have stable bound states in which particle orientations are not aligned in the direction of propulsion. Finally, the bound states found here may have implications for hierarchical self-organization and collective behavior. For instance, Ref. [35] observed that initial formation of immotile head-to-head bound states locally promoted formation of additional bound states in a feedback loop, ultimately leading to phase separation. This mechanism could be studied in the framework of the present work.
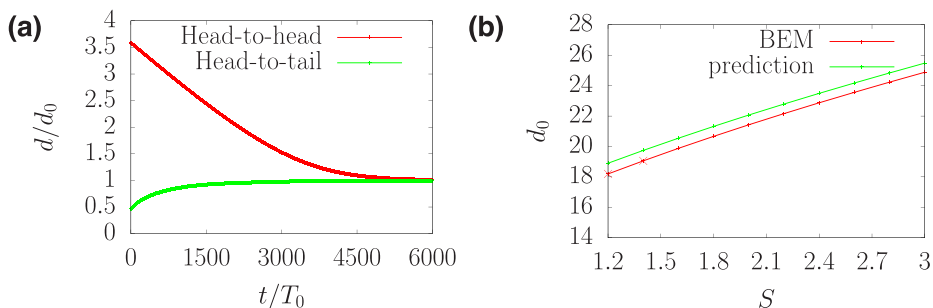

FIG. 5. (a) Separation d for two squirmers forming a stable bound state. For the head-to-tail pair $\Gamma_1 = -0.7$, $\Gamma_2 = -0.8$, $S = 2.2$, and $U = 0.8$, with $x_{2,\text{initial}} = 3$ and $y_{2,\text{initial}} = 10$. For the head-to-head pair, $B_1 = 0.1$, $B_2 = -1$, $\tilde{B} = 1.6833$, and $\Gamma = -0.835$, with $x_{\text{initial}} = 2$ and $y_{\text{initial}} = 55$. The particle parameters correspond to Figs. 2(b) and 4(b), respectively. (b) The predicted and numerically calculated steady separations for head-to-tail pairs with $\Gamma_1 = -0.7$, $\Gamma_2 = -0.8$, $V = 0.8$, and varying S, corresponding to the second row from the bottom in Fig. 4(a). Symbols indicate values of S for which theory and numerics disagree concerning stability.

[1] T. Sanchez, D. T. Chen, S. J. DeCamp, M. Heymann, and Z. Dogic, Spontaneous motion in hierarchically assembled active matter, Nature (London) **491**, 431 (2012).

[2] A. Aubret, M. Youssef, S. Sacanna, and J. Palacci, Targeted assembly and synchronization of self-spinning microgears, Nat. Phys. **14**, 1114 (2018).

[3] A. M. Boymelgreen, T. Balli, T. Miloh, and G. Yossifon, Active colloids as mobile microelectrodes for unified label-free selective cargo transport, Nat. Commun. **9**, 760 (2018).

[4] P. Arora, A. K. Sood, and R. Ganapathy, Emergent stereoselective interactions and self-recognition in polar chiral active ellipsoids, Sci. Adv. **7**, eabd0331 (2021).

[5] J. Palacci, S. Sacanna, A. P. Steinberg, D. J. Pine, and P. M. Chaikin, Living crystals of light-activated colloidal surfers, Science **339**, 936 (2013).

[6] I. Buttinoni, J. Bialké, F. Kümmel, H. Löwen, C. Bechinger, and T. Speck, Dynamical clustering and phase separation in suspensions of self-propelled colloidal particles, Phys. Rev. Lett. **110**, 238301 (2013).

[7] O. Pohl and H. Stark, Dynamic clustering and chemotactic collapse of self-phoretic active particles, Phys. Rev. Lett. **112**, 238303 (2014).

[8] M. E. Cates and J. Tailleur, Motility-induced phase separation, Annu. Rev. Condens. Matter Phys. **6**, 219 (2015).

[9] B. V. Hokmabad, A. Nishide, P. Ramesh, C. Krüger, and C. C. Maass, Spontaneously rotating clusters of active droplets, Soft Matter **18**, 2731 (2022).

[10] A. Bricard, J. Caussin, N. Desreumaux, O. Dauchot, and D. Bartolo, Emergence of macroscopic directed motion in populations of motile colloids, Nature (London) **503**, 95 (2013).

[11] J. Yan, M. Han, J. Zhang, C. Xu, E. Luijten, and S. Granick, Reconfiguring active particles by electrostatic imbalance, Nat. Mater. **15**, 1095 (2016).

[12] A. Kaiser, A. Snezhko, and I. S. Aranson, Flocking ferromagnetic colloids, Sci. Adv. **3**, e1601469 (2017).

[13] K. Han, G. Kokot, O. Tovkach, A. Glatz, I. S. Aranson, and A. Snezhko, Emergence of self-organized multivortex states in flocks of active rollers, Proc. Natl. Acad. Sci. **117**, 9706 (2020).

[14] J. Zhang, R. Alert, J. Yan, N. Wingreen, and S. Granick, Active phase separation by turning towards regions of higher density, Nat. Phys. **17**, 961 (2021).

[15] F. Martínez-Pedrero and P. Tierno, Advances in colloidal manipulation and transport via hydrodynamic interactions, J. Colloid Interface Sci. **519**, 296 (2018).

[16] M. J. Lighthill, On the squirming motion of nearly spherical deformable bodies through liquids at very small reynolds numbers, Commun. Pure Appl. Math. **5**, 109 (1952).

[17] J. R. Blake, A spherical envelope approach to ciliary propulsion, J. Fluid Mech. **46**, 199 (1971).

[18] T. J. Pedley, Spherical squirmers: Models for swimming micro-organisms, IMA J. Appl. Math. **81**, 488 (2016).

[19] T. Ishikawa, M. Simmonds, and T. J. Pedley, Hydrodynamic interaction of two swimming model micro-organisms, J. Fluid Mech. **568**, 119 (2006).

[20] T. Ishikawa and T. Pedley, Diffusion of swimming model micro-organisms in a semi-dilute suspension, J. Fluid Mech. **588**, 437 (2007).

[21] K. Drescher, K. C. Leptos, I. Tuval, T. Ishikawa, T. J. Pedley, and R. E. Goldstein, Dancing Volvox: Hydrodynamic bound states of swimming algae, Phys. Rev. Lett. **102**, 168101 (2009).

[22] I. Llopis and I. Pagonabarraga, Hydrodynamic interactions in squirmer motion: Swimming with a neighbour and close to a wall, J. Non-Newtonian Fluid Mech. **165**, 946 (2010).

[23] K. Ishimoto and E. A. Gaffney, Squirmer dynamics near a boundary, Phys. Rev. E **88**, 062702 (2013).

[24] G.-J. Li and A. M. Ardekani, Hydrodynamic interaction of microswimmers near a wall, Phys. Rev. E **90**, 013010 (2014).

[25] C. Darveniza, T. Ishikawa, T. J. Pedley, and D. R. Brumley, Pairwise scattering and bound states of spherical microorganisms, Phys. Rev. Fluids **7**, 013104 (2022).

[26] V. Magar, T. Goto, and T. J. Pedley, Nutrient uptake by a self-propelled steady squirmer, J. Mech. Appl. Math. **56**, 65 (2003).

[27] S. Michelin and E. Lauga, Optimal feeding is optimal swimming for all péclet numbers, Phys. Fluids **23**, 101901 (2011).

[28] Y. Wang, R. M. Hernandez, D. J. Bartlett, J. M. Bingham, T. R. Kline, A. Sen, and T. E. Mallouk, Bipolar electrochemical mechanism for the propulsion of catalytic nanomotors in hydrogen peroxide solutions, Langmuir **22**, 10451 (2006).

[29] J. R. Howse, R. A. L. Jones, A. J. Ryan, T. Gough, R. Vafabakhsh, and R. Golestanian, Self-motile colloidal particles: From directed propulsion to random walk, Phys. Rev. Lett. **99**, 048102 (2007).

[30] H.-R. Jiang, N. Yoshinaga, and M. Sano, Active motion of a Janus particle by self-thermophoresis in a defocused laser beam, Phys. Rev. Lett. **105**, 268302 (2010).

[31] A. P. Bregulla and F. Cichos, Flow fields around pinned self-thermophoretic microswimmers under confinement, J. Chem. Phys. **151**, 044706 (2019).

[32] M. Popescu, W. Uspal, Z. Eskandari, M. Tasinkevych, and S. Dietrich, Effective squirmer models for self-phoretic chemically active spherical colloids, Eur. Phys. J. E **41**, 145 (2018).

[33] E. Lauga and S. Michelin, Stresslets induced by active swimmers, Phys. Rev. Lett. **117**, 148001 (2016).

[34] H. A. Stone and A. D. T. Samuel, Propulsion of microorganisms by surface distortions, Phys. Rev. Lett. **77**, 4102 (1996).

[35] J. Katuri, R. Poehnl, A. Sokolov, W. Uspal, and A. Snezhko, Arrested-motility states in populations of shape-anisotropic active Janus particles, Sci. Adv. **8**, eabo3604 (2022).

[36] T. M. Squires and M. Z. Bazant, Breaking symmetries in induced-charge electro-osmosis and electrophoresis, J. Fluid Mech. **560**, 65 (2006).

[37] M. S. Kilic and M. Z. Bazant, Induced-charge electrophoresis near a wall, Electrophoresis **32**, 614 (2011).

[38] A. M. Brooks, S. Sabrina, and K. J. Bishop, Shape-directed dynamics of active colloids powered by induced-charge electrophoresis, Proc. Natl. Acad. Sci. **115**, E1090 (2018).

[39] P. Sharan, C. Maslen, B. Altunkeyik, I. Rehor, J. Simmchen, and T. D. Montenegro-Johnson, Fundamental modes of swimming correspond to fundamental modes of shape: Engineering I-, U-, and S-shaped swimmers, Adv. Intell. Syst. **3**, 2100068 (2021).

[40] N. M. Diwakar, G. Kunti, T. Miloh, G. Yossifon, and O. D. Velev, Ac electrohydrodynamic propulsion and rotation of active particles of engineered shape and asymmetry, Curr. Opin. Colloid Interface Sci. **59**, 101586 (2022).

[41] A. Ganguly and A. Gupta, Going in circles: Slender body analysis of a self-propelling bent rod, Phys. Rev. Fluids **8**, 014103 (2023).

[42] M. Theers, E. Westphal, G. Gompper, and R. G. Winkler, Modeling a spheroidal microswimmer and cooperative swimming in a narrow slit, Soft Matter **12**, 7372 (2016).

[43] S. Michelin and E. Lauga, Geometric tuning of self-propulsion for Janus catalytic particles, Sci. Rep. **7**, 42264 (2017).

[44] E. Yariv, Self-diffusiophoresis of slender catalytic colloids, Langmuir **36**, 6903 (2020).

[45] A. Daddi-Moussa-Ider, B. Nasouri, A. Vilfan, and R. Golestanian, Optimal swimmers can be pullers, pushers or neutral depending on the shape, J. Fluid Mech. **922**, R5 (2021).

[46] R. Poehnl and W. Uspal, Phoretic self-propulsion of helical active particles, J. Fluid Mech. **927**, A46 (2021).

[47] A. W. Zantop and H. Stark, Emergent collective dynamics of pusher and puller squirmer rods: Swarming, clustering, and turbulence, Soft Matter **18**, 6179 (2022).

[48] M. Bär, R. Großmann, S. Heidenreich, and F. Peruani, Self-propelled rods: Insights and perspectives for active matter, Annu. Rev. Condens. Matter Phys. **11**, 441 (2020).

[49] B. Felderhof, Stokesian swimming of a prolate spheroid at low Reynolds number, Eur. J. Mech. B Fluids **60**, 230 (2016).

[50] A. M. Leshansky, O. Kenneth, O. Gat, and J. E. Avron, A frictionless microswimmer, New J. Phys. **9**, 145 (2007).

[51] T. Ishikawa and M. Hota, Interaction of two swimming paramecia, J. Exp. Biol. **209**, 4452 (2006).

[52] R. Pöhnl, M. N. Popescu, and W. E. Uspal, Axisymmetric spheroidal squirmers and self-diffusiophoretic particles, J. Phys.: Condens. Matter **32**, 164001 (2020).

[53] R. Archer, A. Campbell, and S. Ebbens, Glancing angle metal evaporation synthesis of catalytic swimming Janus colloids with well defined angular velocity, Soft Matter **11**, 6872 (2015).

[54] M. Lisicki, S. Y. Reigh, and E. Lauga, Autophoretic motion in three dimensions, Soft Matter **14**, 3304 (2018).

[55] W. E. Uspal, M. N. Popescu, S. Dietrich, and M. Tasinkevych, Self-propulsion of a catalytically active particle near a planar wall: From reflection to sliding and hovering, Soft Matter **11**, 434 (2015).

[56] M. N. Popescu, W. E. Uspal, C. Bechinger, and P. Fischer, Chemotaxis of active Janus nanoparticles, Nano Lett. **18**, 5345 (2018).

[57] S. Ghose and R. Adhikari, Irreducible representations of oscillatory and swirling flows in active soft matter, Phys. Rev. Lett. **112**, 118102 (2014).

[58] O. Pak and E. Lauga, Generalized squirming motion of a sphere, J. Eng. Math. **88**, 1 (2014).

[59] B. Felderhof and R. Jones, Stokesian swimming of a sphere at low Reynolds number by helical surface distortion, Phys. Fluids **28**, 073601 (2016).

[60] T. J. Pedley, D. R. Brumley, and R. E. Goldstein, Squirmers with swirl: A model for volvox swimming, J. Fluid Mech. **798**, 165 (2016).

[61] P. S. Burada, R. Maity, and F. Jülicher, Hydrodynamics of chiral squirmers, Phys. Rev. E **105**, 024603 (2022).

[62] D. Saintillan and M. J. Shelley, Orientational order and instabilities in suspensions of self-locomoting rods, Phys. Rev. Lett. **99**, 058102 (2007).

[63] D. Saintillan and M. J. Shelley, Instabilities, pattern formation, and mixing in active suspensions, Phys. Fluids **20**, 123304 (2008).

[64] D. Saintillan and M. Shelley, Active suspensions and their nonlinear models, C. R. Phys. **14**, 497 (2013).

[65] E. Lushi and C. S. Peskin, Modeling and simulation of active suspensions containing large numbers of interacting micro-swimmers, Comput. Construct. **122**, 239 (2013).

[66] S. Kim and S. J. Karrila, *Microhydrodynamics: Principles and Selected Applications* (Dover, New York, 2005).

[67] D. Saintillan, Rheology of active fluids, Annu. Rev. Fluid Mech. **50**, 563 (2018).

[68] See Supplemental Material at http://link.aps.org/supplemental/10.1103/PhysRevFluids.8.113103 for technical discussion of the stresslet tensor, detailed mathematical derivations of results given in the main text, details concerning implementation of the spheroidal squirmer model, and numerical results obtained with the spheroidal squirmer model, which also includes Ref. [74].

[69] C. Pozrikidis, *A Practical Guide to Boundary Element Methods with the Software Library BEMLIB* (CRC Press, Boca Raton, 2002).

[70] G. B. Jeffery, The motion of ellipsoidal particles immersed in a viscous fluid, Proc. R. Soc. Lond. A **102**, 161 (1922).

[71] M. D. Graham, *Microhydrodynamics, Brownian Motion, and Complex Fluids* (Cambridge University Press, Cambridge, 2018), Vol. 58.

[72] Z. Ouyang, Z. Lin, J. Lin, Z. Yu, and N. Phan-Thien, Cargo carrying with an inertial squirmer in a newtonian fluid, J. Fluid Mech. **959**, A25 (2023).

[73] I. L. Claeys and J. F. Brady, Suspensions of prolate spheroids in stokes flow. part 1. dynamics of a finite number of particles in an unbounded fluid, J. Fluid Mech. **251**, 411 (1993).

[74] G. Dassios, M. Hadjinicolaou, and A. Payatakes, Generalized eigenfunctions and complete semiseparable solutions for stokes flow in spheroidal coordinates, Q. Appl. Math. **52**, 157 (1994).